ACS APPLIED MATERIALS & INTERFACES

Research Article

www.acsami.org

Enhanced Microwave Absorption Property of Reduced Graphene Oxide (RGO)-$MnFe_2O_4$ Nanocomposites and Polyvinylidene Fluoride

Xiao-Juan Zhang,[†] Guang-Sheng Wang,*[,†] Wen-Qiang Cao,[‡] Yun-Zhao Wei,[†] Jun-Fei Liang,[†] Lin Guo,*[,†] and Mao-Sheng Cao*[,‡]

[†]Key Laboratory of Bio-Inspired Smart Interfacial Science and Technology of Ministry of Education, School of Chemistry and Environment, Beihang University, Beijing 100191, People's Republic of China

[‡]School of Materials Science and Engineering, Beijing Institute of Technology, Beijing 100081, People's Republic of China

Supporting Information

ABSTRACT: $MnFe_2O_4$ nanoparticles have been synthesized on a large scale by a simple hydrothermal process in a wild condition, and the RGO/$MnFe_2O_4$ nanocomposites were also prepared under ultrasonic treatment based on the synthesized nanoparticles. The absorption properties of $MnFe_2O_4$/wax, RGO/$MnFe_2O_4$/wax and the RGO/$MnFe_2O_4$/PVDF (polyvinylidene fluoride) composites were studied; the results indicated that the RGO/$MnFe_2O_4$/PVDF composites show the most excellent wave absorption properties. The minimum reflection loss of RGO/$MnFe_2O_4$/PVDF composites with filler content of 5 wt % can reach −29.0 dB at 9.2 GHz, and the bandwidth of frequency less than −10 dB is from 8.00 to 12.88 GHz. The wave absorbing mechanism can be attributed to the dielectric loss, magnetic loss and the synergetic effect between RGO+$MnFe_2O_4$, RGO+PVDF and $MnFe_2O_4$+PVDF.

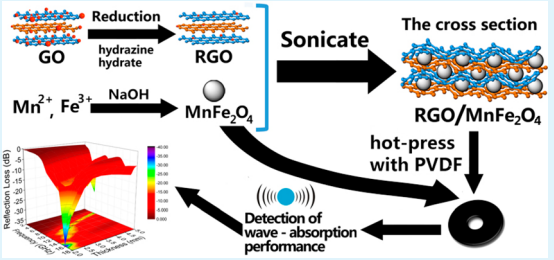

KEYWORDS: *$MnFe_2O_4$ nanoparticles, RGO/$MnFe_2O_4$ nanocomposites, PVDF, wave absorption property*

INTRODUCTION

Recently, many serious electromagnetic interference (EMI) problems have emerged due to the development of GHz telecommunications, military and commercial radar systems and other technical applications. Therefore, great interest has been aroused in electromagnetic wave absorption materials used in the gigahertz (GHz) range.[1,2] An "ideal" electromagnetic wave absorbing material should exhibit low density, tiny thickness, strong wave absorption and broad bandwidth simultaneously.[3−5]

As a typical conventional microwave absorption material, ferrites have been studied extensively.[6−9] Ferrites can attenuate EM waves efficiently because they can make the electromagnetic waves enter availably and avoid the skin effect at high frequencies.[10] For example, Ni et al.[11] fabricated well-dispersed Fe_3O_4 nanocrystals through a wet chemical method and investigated their microwave absorption properties. The minimum calculated reflection loss can reach −21.2 dB at 8.16 GHz with 30 vol % Fe_3O_4 when the matching thickness is 3 mm. Zhao et al.[12] prepared Co-doped Ni−Zn spinel ferrites and reported the single layer $(Ni_{0.4}Co_{0.2}Zn_{0.4})Fe_2O_4$ spinel ferrite absorber attained a reflection loss below −10 dB (90% absorption) at 3.9−11.5 GHz with a thickness of 3 mm, and obtained a minimum reflection loss (RL) value of −17.01 dB at 6.1 GHz. Peng et al.[13] studied the microwave absorption property of silver nanoparticles coated with $Ni_{0.5}Zn_{0.5}Fe_2O_4$ spinel ferrites and polyurethane in the range of 2−15 GHz. The results showed that the matched frequency for reflection loss exceeded −25 dB was 9.0 GHz. However, the high density and poor environmental stability of ferrite absorbers will restrict their wide applications as microwave absorbents. Except for these two shortcomings, traditional ferrites have narrow wave absorbing band and poor flexibility.[14,15]

In the past few decades, the spinel ferrites have been used as absorbing materials in different forms.[16] As a common spinel ferrite material, manganese ferrite ($MnFe_2O_4$) has been widely utilized in magnetic recording and microwave absorption fields.[17] Recently, magnetic nanocomposites have become a promising EM wave absorbing material due to their superiorities of low cost, light weight, design flexibility, and good microwave properties.[18] Hosseini et al.[19] investigated the wave absorbing properties of the conductive polyaniline (PANi)-manganese ferrite ($MnFe_2O_4$) nanocomposite scattering in resin acrylic coating with the thickness of 1.4 mm in the frequency range of 8−12 GHz. The minimum reflection loss value was −15.3 dB at 10.4 GHz. In addition, this research group also synthesized conductive polypyrrole (PPy)−manganese ferrite ($MnFe_2O_4$) nanocomposites and found that a minimum reflection loss of the nanocomposite powders dispersing in resin acrylic coating can reach −12 dB at 11.3 GHz with the coating thickness of 1.5 mm.[20]

Received: February 10, 2014
Accepted: April 29, 2014
Published: April 29, 2014

   dx.doi.org/10.1021/am500862g | ACS Appl. Mater. Interfaces 2014, 6, 7471−7478

Compared with traditional microwave absorption materials, reduced graphene oxide (RGO) has been applied as a new wave absorbing material because of its desirable physical and chemical properties. Because RGO is nonmagnetic, its microwave absorption properties mostly owe to the dielectric loss.[21,22] Singh et al.[23] investigated that nitrile butadiene rubber composites with 10 wt % reduced graphene oxide exhibited a minimum reflection loss of −57 dB at 9.6 GHz with a thickness of 3 mm and had a wide frequency range of 7.5−12 GHz when RL <−10 dB. Novel $NiFe_2O_4$ nanorod−graphene composites were synthesized by Fu et al.[24] A minimum reflection loss of −29.2 dB appeared at 16.1 GHz in the composites when the thickness was 2.0 mm, and the effective absorption frequency (RL <−10 dB) ranged from 13.6 to 18.0 GHz.

Just like many other researchers studied, the combination of complex oxides with other domains will attract broad research interest for the design of new functional materials. For example, Guo et al.[25] fabricated complex oxide−noble metal hybrids (such as Au−$CoFe_2O_4$ and Au−$SrTiO_3$ nanoparticles) and studied their opticle, magnetic and photocatalytic properties. Zheng et al.[26] reported a nanostrctured $BaTiO_3$−$CoFe_2O_4$ ferroelectromagnet on the coupling between ferroelectric and magnetic order parameters. This composite facilitated the interconversion of energies stored in electric and magnetic fields and played an important role in many devices, such as transducers, field sensors, etc. Ren and Wuttig[27] fabricated a composite formed of Fe_3O_4/$CoFe_2O_4$ nanoparticles inserted into a PZT matrix and measured the variation in the magnetic moment based on the applied electric field. When the smallest particle size reached 5 nm, the coercive field was as low as 25 Oe and the inverse ME_E voltage coefficient was as high as $(10.1\ V/cm\ Oe)^{-1}$. In addition, Peng et al.[28] synthesized manganese ferrite/graphene oxide nanocomposites (MGONCs) and found MGONCs showed an excellent biocompatibility that was fit for biomedical applications.

Therefore, to further investigate the wave absorption property of spinel $MnFe_2O_4$, we synthesized $MnFe_2O_4$ nanoparticles by a simple hydrothermal process and combined them with reduced graphene oxide (RGO) to form RGO/$MnFe_2O_4$ nanocomposites. And on the basis of our previous research,[29−32] we use polyvinylidene fluoride (PVDF) instead of wax as a matrix. PVDF is a typical dielectric material, and its simple chemical structure (−CH_2−CF_2−) gives the molecular chain both high flexibility and some stereochemical constraint. At the same time, the synergic effect between nanomaterials, RGO and PVDF would enhance their wave absorption properties. Thus, we prepared RGO/$MnFe_2O_4$ nanocomposites and first investigated their wave absorption properties with PVDF.

EXPERIMENTAL SECTION

Preparation of $MnFe_2O_4$ Nanoparticles. The chemical reagents used in this work were manganese chloride tetrahydrate ($MnCl_2\cdot 4H_2O$), ferric chloride hexahydrate ($FeCl_3\cdot 6H_2O$) and sodium hydroxide (NaOH). In a typical synthesis, $MnCl_2\cdot 4H_2O$ (0.05 M) and $FeCl_3\cdot 6H_2O$ (0.1 M) were dissolved in water at room temperature, respectively. Then the homogeneous suspension was transferred into a Teflon-lined stainless steel autoclave (100 mL). Sodium hydroxide (1.76 g) dissolved with 10.0 mL of deionized water was added dropwise into the Teflon-lined stainless autoclave slowly. A brown precipitate formed immediately. After a reaction at 140 °C for 12 h, the solution was cooled to room temperature. Then the resultant brown product was washed with deionized water and absolute ethanol for several times and finally dried at 60 °C for 12 h for further characterization.

Preparation of RGO/$MnFe_2O_4$ Nanocomposites. Graphite oxide was synthesized by a modified Hummers method.[33] The typical synthesis process was the same with our pervious reported.[32] To obtain RGO/$MnFe_2O_4$ nanocomposites, 50 mg of $MnFe_2O_4$ nanoparticles was added to RGO suspension and sonicated for another 2 h. The black precipitates was isolated by centrifugation, washed with absolute ethanol and finally dried at 60 °C for 12 h.

Characterization. XRD measurements were carried out using an X-ray diffractometer (D/MAX-1200, Rigaku Denki Co. Ltd., Japan). The XRD patterns with Cu Ka radiation (λ = 1.5406 Å, 40 kV, 40 mA) were recorded in the range of 2θ = 5°−90°. Scanning electron microscopy (SEM) images were acquired on a FEI Quanta 250 field-emission gun environmental scanning electron microscope at 15 kV. Raman spectra were obtained from 200 to 2000 cm^{-1} by a LabRAM HR800 laser Raman spectroscopy (HORIBA Jobin Yvon CO. Ltd., France) using a 632.5 nm argon ion laser. FTIR spectra were recorded on FTIR spectrometer-733 (iN10MX). Thermogravimetric (TG) analysis was performed in air using a Pyris Diamond TG analyzer (PerkinElemer Inc., U.S.A). The samples were heated from 20 to 800 °C at 5 °C min^{-1}. The magnetic properties were carried out at 300 K on a Quantum Design superconducting quantum interference device (SQUID) magnetometer (MPMS-7).

EM Absorption Measurement. The composites used for EM absorption measurement were prepared through mixing the products with wax and PVDF in different mass percentages, respectively. For $MnFe_2O_4$/wax and RGO/$MnFe_2O_4$/wax composites, 10 wt % $MnFe_2O_4$ or RGO/$MnFe_2O_4$ nanoparticles was mixed with wax uniformly by sonicating at 60 °C. And for $MnFe_2O_4$/PVDF and RGO/$MnFe_2O_4$/PVDF composites, PVDF was first dissolved in *N,N*-dimethylformamide (DMF) at room temperature. Then different contents of $MnFe_2O_4$ or RGO/$MnFe_2O_4$ nanoparticles were added and poured into glassy Petri dishes after sonicating the dispersion uniformly at room temperature. Finally, it was dried at 100 °C for 3 h. after that, the mixtures were pressed into cylindrical-shaped specimens (Φ_{out} = 7.00 mm and Φ_{in} = 3.04 mm). The complex permittivity and permeability values were measured with coaxial wire method in the frequency range of 2−18 GHz with the network analyzer (Anritsu 37269D).

RESULTS AND DISCUSSION

Figure 1 shows the SEM pictures of $MnFe_2O_4$ nanoparticles and RGO/$MnFe_2O_4$ nanocomposites. From Figure 1a,b, it indicates that the average diameter of $MnFe_2O_4$ nanoparticle is about in the range of 50−80 nm. The granular structure is the exclusive morphology and the products can be prepared on a large scale. Moreover, as shown in Figure 1c,d, the $MnFe_2O_4$ nanoparticles have been coated by RGO absolutely.

To investigate how the RGO/$MnFe_2O_4$ nanocomposites disperse in PVDF, the FESEM image and elemental mappings of RGO/$MnFe_2O_4$/PVDF composites are displayed in Figure 2. The elemental mapping images of Mn, Fe, O and C indicate that the RGO/$MnFe_2O_4$ nanocomposites disperse homogeneously in PVDF. The good dispersion of these nanocomposites in PVDF may be helpful for the wave absorption properties.

Figure 3a shows the typical XRD patterns of $MnFe_2O_4$ nanoparticles, RGO/$MnFe_2O_4$ nanocomposites, RGO/$MnFe_2O_4$/PVDF membrane and PVDF. From the XRD pattern of $MnFe_2O_4$ nanoparticles, it can be seen that all the diffraction peaks are readily indexed to the face-centered cubic structure of jacobsite ferrite (JCPDS No. 10-0319). The narrow sharp peaks confirm that the $MnFe_2O_4$ particles are highly crystallized. Moreover, the XRD pattern of RGO/$MnFe_2O_4$ nanocomposites is almost the same as that of $MnFe_2O_4$ nanoparticles. In addition, the absence of X-ray diffraction

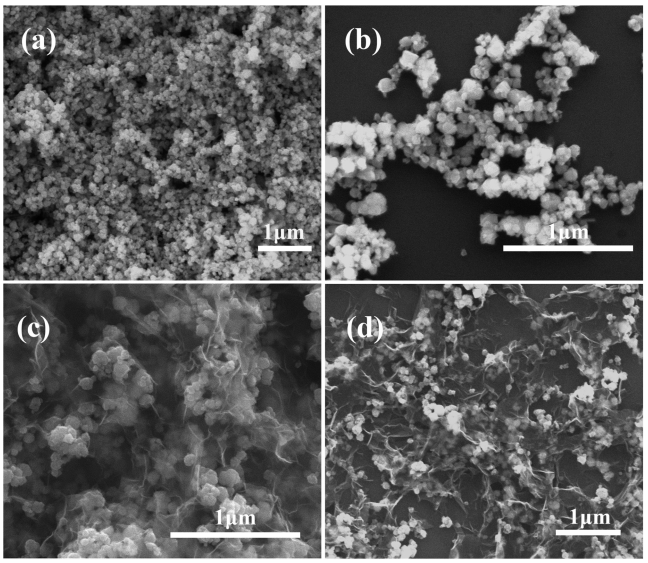

Figure 1. SEM pictures of $MnFe_2O_4$ nanoparticles (a,b) and RGO/$MnFe_2O_4$ nanocomposites (c,d).

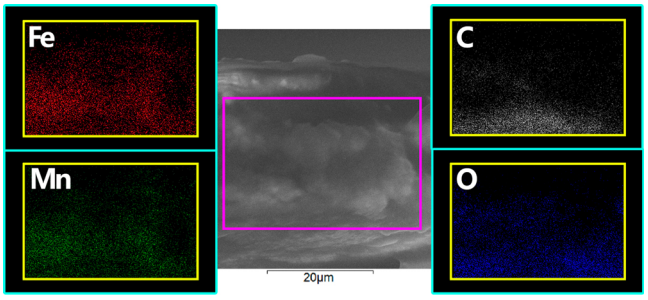

Figure 2. FESEM image of the fracture section of RGO/$MnFe_2O_4$/PVDF membrane and corresponding elemental mapping images of Fe, C, Mn and O.

peak for GO around 10° in RGO/$MnFe_2O_4$ nanocomposites indicate that GO can be reduced to RGO effectively. And the conventional stacking peak of graphite at around 26° also disappears (as shown in Figure S1, Supporting Information), demonstrating that the RGO nanosheets do not stack together and disperse on the surface of $MnFe_2O_4$ nanoparticles homogeneously.[34,35] Compared with the XRD patterns of RGO/$MnFe_2O_4$ nanocomposites and PVDF, all the diffraction peaks of $MnFe_2O_4$ and PVDF exsit in the RGO/$MnFe_2O_4$/PVDF membrane, indicating that the RGO/$MnFe_2O_4$ nanocomposites disperse in PVDF effectively. The results of FTIR test will further confirm the GO is reduced to RGO successfully. As shown in Figure 3b, from the FTIR spectra of GO, the broad band with the range from 3000 to 3600 cm^{-1} is attributed to O—H stretching vibrations of carboxyl groups and the absorbed water molecules. The characteristic peak appears at 1730 and 1622 cm^{-1} are the C═O stretching vibration and the C═C skeletal stretching vibration, respectively. For O—H of carboxylic groups, the flexural vibration shows at 1420 cm^{-1}. The peak at 1220 cm^{-1} can be assigned to the epoxy C—O stretching vibration. While the alkoxy C—O stretching vibration appears at 1040 cm^{-1}.[36] After reduction by hydrazine hydrate, the peaks for oxygen functional groups decrease dramatically. This indicates that GO has been translated to RGO effectively. TG analysis curves of the RGO/$MnFe_2O_4$ nanocomposites were used to quantify the amount of RGO in the composites. The TG curves (shown in Figure 3c) demonstrate that the $MnFe_2O_4$ nanoparticles remain stable over the entire temperature range and the rapid weight loss of RGO/$MnFe_2O_4$ nanocomposites appears between 350 to 500 °C, which is attributed to the oxidation of carbon. On the basis of weight loss rate, the amount of RGO in the composites is about 27 wt %. The Raman spectroscopy is an important tool to explore the structural properties of synthesized materials. The Raman spectra curves of GO and RGO/$MnFe_2O_4$ nanocomposites are shown in Figure 3d. GO displays a D

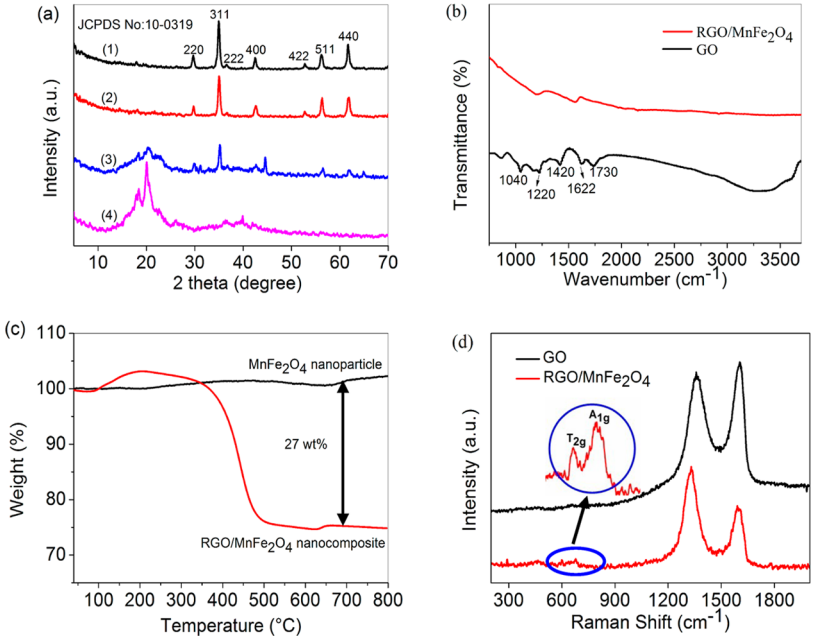

Figure 3. (a) XRD patterns of (1) $MnFe_2O_4$ nanoparticles, (2) RGO/$MnFe_2O_4$ nanocomposites, (3) RGO/$MnFe_2O_4$/PVDF membrane, (4) PVDF; (b) FTIR spectrum of the GO and RGO/$MnFe_2O_4$ nanocomposites; (c) TG curve of the $MnFe_2O_4$ nanoparticles and RGO/$MnFe_2O_4$ nanocomposites; (d) Raman spectrum of the GO and RGO/$MnFe_2O_4$ nanocomposites.

dx.doi.org/10.1021/am500862g | ACS Appl. Mater. Interfaces 2014, 6, 7471−7478

band at 1359 cm^{-1} and a G band at 1604 cm^{-1}, whereas the corresponding bands for RGO are 1329 and 1592 cm^{-1}, respectively. It can be obviously observed that the G band of RGO red-shifted from 1604 to 1592 cm^{-1}, which is due to the recovery of the hexagonal network of carbon atom. And the RGO shows relatively higher intensity of D to G band (1.55) than that of GO (0.93), indicating the formation of new and smaller sp^2 domains during the reduction. In addition, as shown in the blue circles, the peaks appearing at 447 and 617 cm^{-1} are assigned to the T_{2g} and A_{1g} modes of $MnFe_2O_4$. Mode A_{1g} is owing to symmetric stretching of oxygen atoms at tetrahedral site, whereas mode T_{2g} represents the characteristic of the octahedral sites.[37−39]

The magnetic property is important to investigate the electromagnetic wave absorption properties; the magnetic properties of the as-synthesized $MnFe_2O_4$ nanoparticles and RGO/$MnFe_2O_4$ nanocomposites were first measured at room temperature. As observed in Figure 4, both the two samples

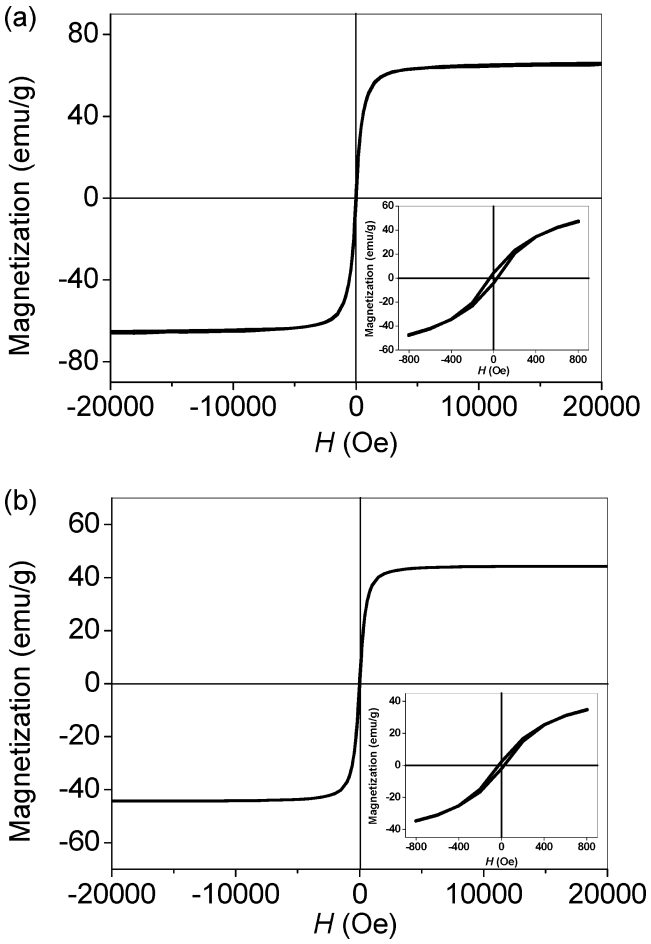

Figure 4. Hysteresis loops of $MnFe_2O_4$ nanoparticles at room temperature (a) and RGO/$MnFe_2O_4$ nanocomposites (b). The insets are amplified views of the hysteresis loops at low applied fields.

show a typical hysteresis loop in their magnetic behavior. The insets display the magnified views of the hysteresis loops at low applied fields. The hysteresis loop of $MnFe_2O_4$ nanoparticles indicates that it is a typical soft magnetic material. The saturation magnetization (M_s), remanent magnetization (M_r), and coercivity (H_c) values of $MnFe_2O_4$ nanoparticles and RGO/$MnFe_2O_4$ nanocomposites are 65.1 emu/g, 4.37 emu/g, 35.5 Oe and 44.2 emu/g, 2.21 emu/g, 24.6 Oe, respectively. The difference in M_s values of these two nanoparticles may be attributed to the introduction of RGO.[40] Additionally, both the $MnFe_2O_4$ nanoparticles and RGO/$MnFe_2O_4$ nanocomposites express typical ferromagnetic behavior, as shown in Figure S2 (Supporting Information).

To investigate the electromagnetic wave absorption properties of $MnFe_2O_4$ nanoparticles and RGO/$MnFe_2O_4$ nanocomposites, various contents of the products were blended with wax or PVDF to form composites via a hot-press process. The frequency dependence relative permittivity and permeability for several materials are shown in Figure 5. The real permittivity (ε') and real permeability (μ') represent the storage ability of electromagnetic energy, whereas the imaginary permittivity (ε'') and imaginary permeability (μ'') are connected with the energy dissipation and magnetic loss, respectively.[41] It is observed that the values of ε' and ε'' for RGO/$MnFe_2O_4$+PVDF composites are much larger than that of $MnFe_2O_4$+wax, RGO/$MnFe_2O_4$+wax and $MnFe_2O_4$+PVDF composites. Moreover, the variation tendency of μ' and μ'' for these composites are basically the same. The negative μ'' values appear in $MnFe_2O_4$+wax, RGO/$MnFe_2O_4$+wax and $MnFe_2O_4$+PVDF composites, which signifies the magnetic energy radiate out without any absorption.[42]

To study the microwave absorption property, the reflection loss (RL) of the electromagnetic radiation was calculated. On the basis of the measured data of permittivity and permeability, reflection loss (RL) usually can be calculated by the following expression:[43]

$$R = 20\log\left|\frac{Z_{in} - 1}{Z_{in} + 1}\right| \quad (1)$$

where Z_{in} is the input characteristic impedance, which can be expressed as[44]

$$Z_{in} = \sqrt{\frac{\mu_r}{\varepsilon_r}}\tanh\left[j\left(\frac{2f\pi d}{c}\right)\sqrt{\mu_r\varepsilon_r}\right] \quad (2)$$

where ε_r and μ_r are the complex permittivity and permeability of the absorber, respectively, f is the frequency, d is the thickness of the absorbent and c is the velocity of light in free space.

From the values of dielectric loss and magnetic loss (shown in Figure 6), it can be concluded that the magnetic loss values of $MnFe_2O_4$+wax and $MnFe_2O_4$+PVDF composites are higher than their dielectric loss values. Therefore, the main loss mechanism for these two composites is magnetic loss rather than dielectric loss.[45] The maximum values are 0.13 (12 GHz) and 0.32 (10.16 GHz), which are in accordance with the reflection loss peak (shown in Figure 7a). However, after combining RGO and PVDF with $MnFe_2O_4$ nanoparticles, the dielectric loss values are higher than the magnetic loss values. The dielectric loss values of 10 wt % $MnFe_2O_4$+PVDF and 10 wt % RGO/$MnFe_2O_4$+PVDF indicate that the dielectric loss values are improved dramatically after combining with RGO.[46] Similarly, the dielectric loss values of 10 wt % RGO/$MnFe_2O_4$+PVDF are much higher than that of 10 wt % RGO/$MnFe_2O_4$+wax, which demonstrates that PVDF can influence the dielectric behaviors of composites effectively.[47] The causes for dielectric loss include interfacial polarization and electronic dipole polarization. Interface polarization arises when the neighboring phases differ from each other in a dielectric constant, conductivity, or both, at testing frequencies.[48] In

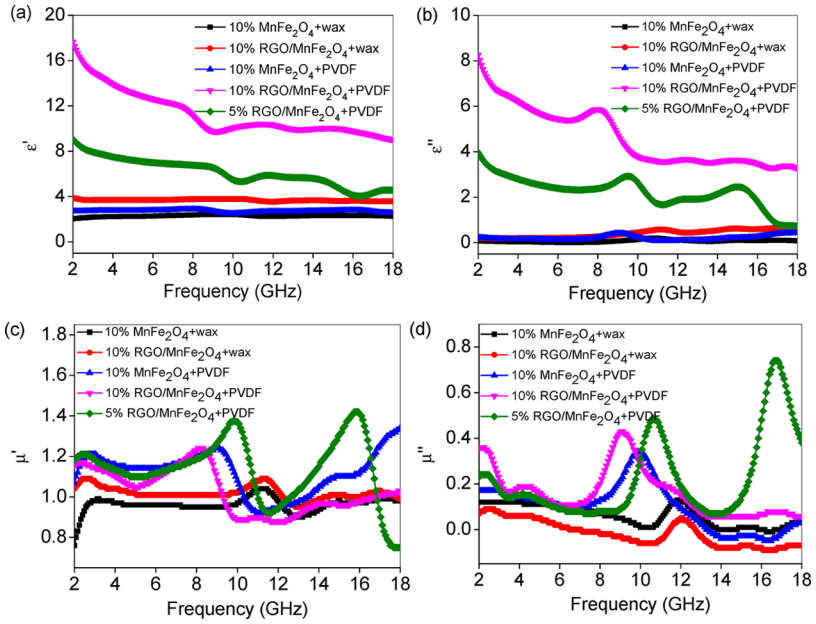

Figure 5. Frequency dependence of (a) real and (b) imaginary parts of relative complex permittivity; (c) real and (d) imaginary parts of relative complex permeability of samples.

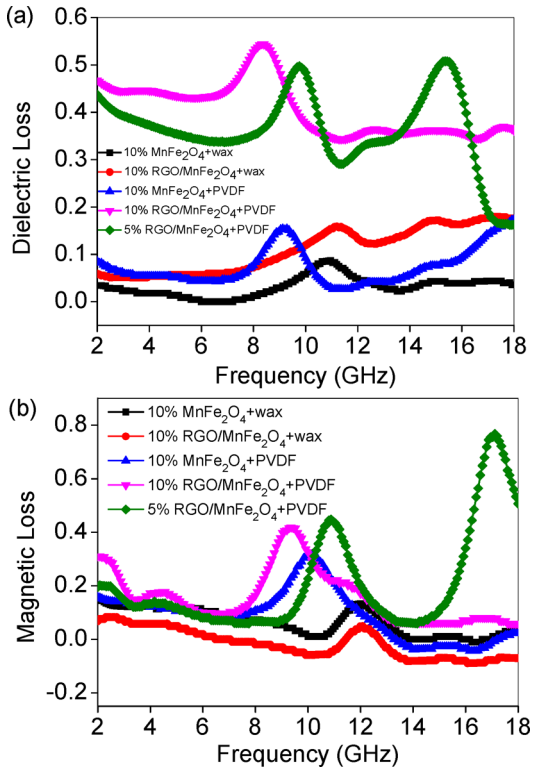

Figure 6. Frequency dependence of dielectric loss (a) and magnetic loss (b) of samples.

RGO/$MnFe_2O_4$/PVDF composites, the interface is caused by RGO, $MnFe_2O_4$ and PVDF. As demonstrated before, RGO is a new microwave absorbing material due to its desirable physical and chemical properties.[49] And because PVDF is a strong dipole material due to the existence of electrophilic fluorine in its molecular structure. Therefore, it may cause electronic dipole polarization. These all illustrate that RGO and PVDF are beneficial to microwave absorption properties.[22,49−51] However, the maximum dielectric loss values for these composites are almost same, and the frequency of the maximum peak is not consistent with that of the reflection loss peak. Therefore, the main loss mechanism for RGO/$MnFe_2O_4$+wax and RGO/$MnFe_2O_4$+PVDF composites includes both dielectric loss and magnetic loss.

On the basis of Van Der Zaag's research achievement,[52] the magnetic dissipation of classified ferrite contains eddy current loss, hysteresis loss, residual loss, intragranular domain wall loss and ferromagnetic resonance loss. For RGO/$MnFe_2O_4$/PVDF composites, magnetic loss is caused by the time lag of the magnetization vector **M**, behind the magnetic field vector **H**. There is a reversible rotational magnetization process when a weak magnetic field is applied to RGO/$MnFe_2O_4$ nanocomposites, just as the hysteresis loop curve shows in Figure 4b. The reversible rotation of the magnetization vector will make the permeability in high frequency.[53] Furthermore, as $MnFe_2O_4$ is a ferromagnetic material, so the eddy current effect is an important factor to influence the microwave absorption property at high frequencies. The eddy current loss can be calculated by the following equation:

$$\mu'' \approx 2\pi\mu_0(\mu')^2\sigma d^2 f/3 \quad (3)$$

where μ_0 (H·m^{-1}) is the permeability in a vacuum and σ (S·cm^{-1}) is the electrical conductivity. If the reflection loss is caused by the eddy current loss effect, the values of C_0 ($C_0 = \mu''(\mu')^{-2}f^{-1}$) are constant when the frequency varies. Figure S3 (Supporting Information) shows the C_0−f curve of 5 wt % RGO/$MnFe_2O_4$/PVDF composites. It can be observed that the value of C_0 is almost constant within the frequency range from 6 to 10 GHz and from 13 to 15 GHz, which indicates that the RGO/$MnFe_2O_4$/PVDF composites have an obvious eddy current effect for the microwave energy dissipation. The enhancement of anisotropic energy (H_a) is another mechanism for magnetic loss in RGO/$MnFe_2O_4$/PVDF composites. It can be expressed in the following equation:

$$H_a = 4|K_1|/3\mu_0 M_s \quad (4)$$

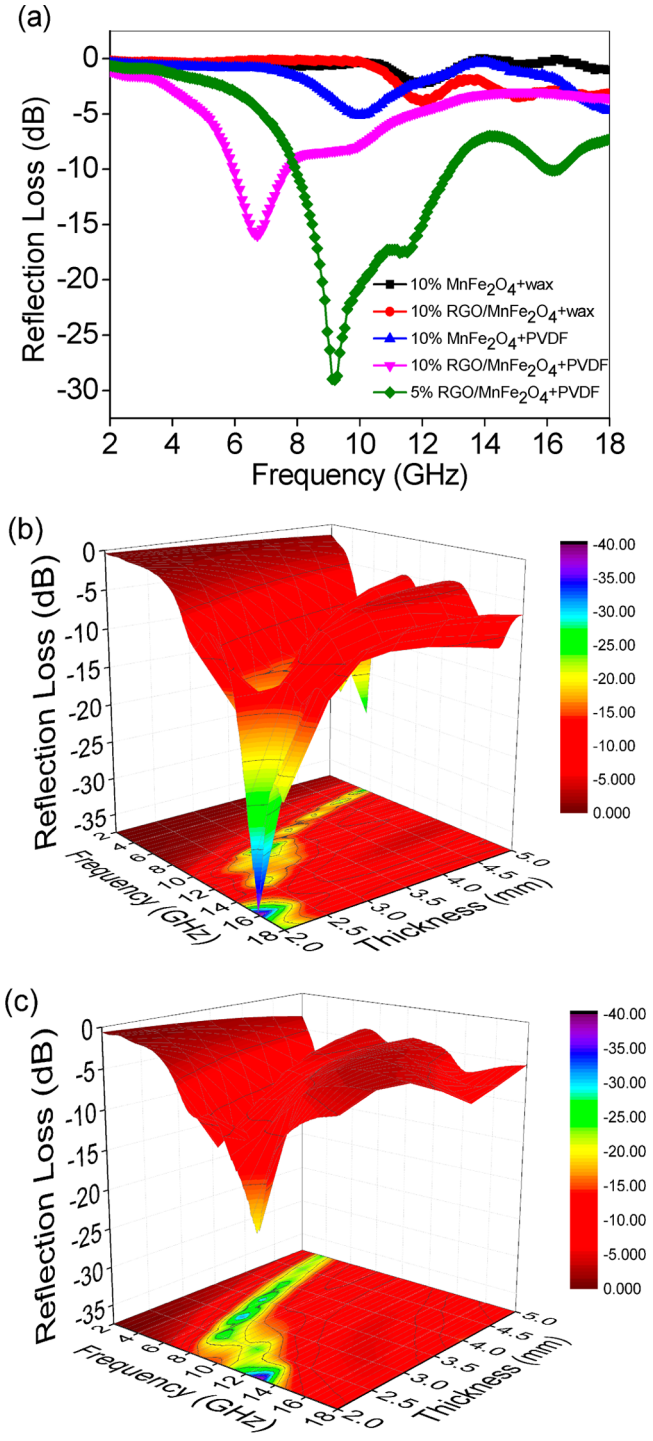

Figure 7. (a) Reflection coefficient of the products with a thickness of 3.0 mm in the range of 2−18 GHz. Three-dimensional presentations of the reflection loss of (b) RGO/$MnFe_2O_4$+PVDF composites the filler content of 5 wt %; (c) RGO/$MnFe_2O_4$+PVDF composites with the filler content of 10 wt %.

where $|K_1|$ is the anisotropic coefficient and M_s is the saturation magnetization. As shown in Figure 4, the M_s value of RGO/$MnFe_2O_4$ nanocomposites is lower than that of $MnFe_2O_4$ nanoparticles. Thus, the anisotropic energy of RGO/$MnFe_2O_4$/PVDF composites is higher. The higher anisotropic energy is conductive to the improvement of EM absorption performance, particularly at high frequencies.[54,55] In addition, the synergetic effect between RGO+$MnFe_2O_4$, RGO+PVDF and $MnFe_2O_4$+PVDF could also enhance the wave absorption abilities, as indicated in our previous research.[29−31] And the distinction of complex permittivity among RGO, $MnFe_2O_4$ and PVDF would generate interface scattering, leading to more wave absorption.[24]

As observed in Figure 7, the RGO/$MnFe_2O_4$+PVDF composites show enhanced wave absorption properties. Figure 7a shows the theoretical reflection loss (RLs) of composites $MnFe_2O_4$+wax, RGO/$MnFe_2O_4$+wax, $MnFe_2O_4$+PVDF and RGO/$MnFe_2O_4$+PVDF at a thickness of 3.0 mm in the range of 2−18 GHz. It is observed that the reflection loss value of the RGO/$MnFe_2O_4$+PVDF composite is much higher than that of other composites. The minimum reflection loss of the RGO/$MnFe_2O_4$+PVDF composite reaches −29.0 dB at 9.2 GHz with a filler content of only 5 wt % with a thickness of 3.0 mm, and the frequency bandwidth less than −10 dB is from 8.00 to 12.88 GHz. Figure 7b,c shows the three-dimensional presentations of calculated theoretical RLs of the RGO/$MnFe_2O_4$+PVDF composites at various thicknesses (2−5 mm) in the frequency range of 2−18 GHz with the filler loading of 5 and 10 wt %, respectively. This indicates that the microwave absorbing ability of the RGO/$MnFe_2O_4$+PVDF composite at different frequencies can be adjusted by controlling the thickness of the absorbents. Except for the enhanced wave absorption properties, the RGO/$MnFe_2O_4$+PVDF membrane is still as flexible as the pure PVDF and can be cut into different shapes (Figure S4, Supporting Information).

CONCLUSION

Magnetic $MnFe_2O_4$ nanoparticles and RGO/$MnFe_2O_4$ nanocomposites have been fabricated on a large scale via a simple process. The results indicated that the RGO/$MnFe_2O_4$+PVDF composites possess excellent wave absorption properties. For the composites with a filler content of 5 wt %, the minimum reflection loss of RGO/$MnFe_2O_4$+PVDF composite reaches −29.0 dB at 9.2 GHz, and the composites show a relative wide frequency band of 8.00−12.88 GHz (RL <−10 dB). The main microwave absorbing mechanism of the RGO/$MnFe_2O_4$+PVDF composite is the dielectric loss, magnetic loss and the synergetic effect between RGO+$MnFe_2O_4$, RGO +PVDF and $MnFe_2O_4$+PVDF. Therefore, it turned out that the composites are promising materials in microwave absorption areas.

ASSOCIATED CONTENT

Supporting Information

XRD data of graphite and graphene oxide, ferromagnetic property of $MnFe_2O_4$ nanoparticles and RGO/$MnFe_2O_4$ nanocomposites, C_0−f curve of 5 wt % RGO/$MnFe_2O_4$/PVDF composites and flexibility of RGO/$MnFe_2O_4$/PVDF membrane. This material is available free of charge via the Internet at http://pubs.acs.org/.

AUTHOR INFORMATION

Corresponding Authors

*Guang-Sheng Wang. E-mail: wanggsh@buaa.edu.cn.
*Lin Guo. E-mail: guolin@buaa.edu.cn.
*Mao-Sheng Cao. E-mail: caomaosheng@bit.edu.cn.

Notes

The authors declare no competing financial interest.

■ ACKNOWLEDGMENTS

This project was financially supported by the National Basic Research Program of China (2010CB934700) and the National Natural Science Foundation of China (Nos. 51102223, 5072508 and 51132002).

■ REFERENCES

(1) Zhu, W.; Wang, L.; Zhao, R.; Ren, J.; Lu, G.; Wang, Y. Electromagnetic and Microwave-absorbing Properties of Magnetic Nickel Ferrite Nanocrystals. *Nanoscale* **2011**, *3*, 2862−2864.

(2) Guo, J.; Wang, X.; Liao, X.; Zhanga, W.; Shi, B. Skin Collagen Fiber-Biotemplated Synthesis of Size-Tunable Silver Nanoparticle-Embedded Hierarchical Intertextures with Lightweight and Highly Efficient Microwave Absorption Properties. *J. Phys. Chem. C* **2012**, *116*, 8188−8195.

(3) Liu, J.; Che, R.; Chen, H.; Zhang, F.; Xia, F.; Wu, Q.; Wang, M. Microwave Absorption Enhancement of Multifunctional Composite Microspheres with Spinel Fe_3O_4 Cores and Anatase TiO_2 Shells. *Small* **2012**, *8*, 1214−1221.

(4) Guo, J.; Wu, H.; Liao, X.; Shi, B. Facile Synthesis of Size-Controlled Silver Nanoparticles Using Plant Tannin Grafted Collagen Fiber As Reductant and Stabilizer for Microwave Absorption Application in the Whole Ku Band. *J. Phys. Chem. C* **2011**, *115*, 23688−23694.

(5) Kong, L.; Yin, X.; Zhang, Y.; Yuan, X.; Li, Q.; Ye, F.; Cheng, L.; Zhang, L. Electromagnetic Wave Absorption Properties of Reduced Graphene Oxide Modified by Maghemite Colloidal Nanoparticle Clusters. *J. Phys. Chem. C* **2013**, *117*, 19701−19711.

(6) Kong, J.; Liu, J.; Wang, F.; Luan, L.; Itoh, M.; Machida, K. I. Electromagnetic Wave Absorption Properties of Fe_3O_4 Octahedral Nanocrystallines in Gigahertz Range. *Appl. Phys. A: Mater. Sci. Process.* **2011**, *105*, 351−354.

(7) Kagotani, T.; Fujiwara, D.; Sugimoto, S.; Inomata, K.; Homma, M. Enhancement of GHz Electromagnetic Wave Absorption Characteristics in Aligned M-type Barium Ferrite $Ba_{1-x}La_xZn_xFe_{12-x-y}(Me_{0.5}Mn_{0.5})yO_{19}$ (x=0.0−0.5; y=1.0−3.0, Me: Zr, Sn) by Metal Substitution. *J. Magn. Magn. Mater.* **2004**, *272*−*276*, E1813−E1815.

(8) Dosoudil, R.; Franek, J.; Slama, J.; Usakova, M.; Gruskova, A. Electromagnetic Wave Absorption Performances of Metal Alloy/Spinel Ferrite/Polymer Composites. *IEEE Trans. Magn.* **2012**, *48*, 1524−1527.

(9) Tyagi, S.; Baskey, H. B.; Agarwala, R. C.; Agarwala, V.; Shami, T. C. Development of Hard/soft Ferrite Nanocomposite for Enhanced Microwave Absorption. *Ceram. Int.* **2011**, *37*, 2631−2641.

(10) Fu, W.; Liu, S.; Fan, W.; Yang, H.; Pang, X.; Xu, J.; Zou, G. Hollow Glass Microspheres Coated with $CoFe_2O_4$ and its Microwave Absorption Property. *J. Magn. Magn. Mater.* **2007**, *316*, 54−58.

(11) Ni, S.; Lin, S.; Pan, Q.; Yang, F.; Huang, K.; He, D. Hydrothermal Synthesis and Microwave Absorption Properties of Fe_3O_4 Nanocrystals. *J. Phys. D: Appl. Phys.* **2009**, *42*, 055004.

(12) Zhao, D. L.; Lv, Q.; Shen, Z. M. Fabrication and Microwave Absorbing Properties of Ni−Zn Spinel Ferrites. *J. Alloys Compd.* **2009**, *480*, 634−638.

(13) Peng, C. H.; Wang, H. W.; Kan, S. W.; Shen, M. Z.; Wei, Y. M.; Chen, S. Y. Microwave Absorbing Materials Using Ag−NiZn Ferrite Core−shell Nanopowders as Fillers. *J. Magn. Magn. Mater.* **2004**, *284*, 113−119.

(14) Khan, K. Microwave Absorption Properties of Radar Absorbing Nanosized Cobalt Ferrites for High Frequency Applications. *J. Supercond. Novel Magn.* **2014**, *27*, 453−461.

(15) Sunny, V.; Kurian, P.; Mohanan, P.; Joy, P. A.; Anantharaman, M. R. A Flexible Microwave Absorber Based on Nickel Ferrite Nanocomposite. *J. Alloys Compd.* **2010**, *489*, 297−303.

(16) Yalçın, O.; Bayrakdar, H.; Özüm, S. Spin-flop Transition, Magnetic and Microwave Absorption Properties of α-Fe_2O_4 Spinel Type Ferrite Nanoparticles. *J. Magn. Magn. Mater.* **2013**, *343*, 157−162.

(17) Xiao, H. M.; Liu, X. M.; Fu, S. Y. Synthesis, Magnetic and Microwave Absorbing Properties of Core-shell Structured $MnFe_2O_4$/TiO_2 Nanocomposites. *Compos. Sci. Technol.* **2006**, *66*, 2003−2008.

(18) Shimba, K.; Tezuka, N.; Sugimoto, S. Magnetic and Microwave Absorption Properties of Polymer Composites with Amorphous Fe-B/Ni−Zn Ferrite Nanoparticles. *Mater. Sci. Eng., B* **2012**, *177*, 251−256.

(19) Hosseini, S. H.; Mohseni, S. H.; Asadnia, A.; Kerdari, H. Synthesis and Microwave Absorbing Properties of Polyaniline/$MnFe_2O_4$ Nanocomposite. *J. Alloys Compd.* **2011**, *509*, 4682−4687.

(20) Hosseini, S. H.; Asadnia, A. Synthesis, Characterization, and Microwave-Absorbing Properties of Polypyrrole/$MnFe_2O_4$ Nanocomposite. *J. Nanomater.* **2012**, *2012*, 1−6.

(21) Liu, P.; Huang, Y.; Wang, L.; Zong, M.; Zhang, W. Hydrothermal Synthesis of Reduced Graphene Oxide−Co_3O_4 Composites and the Excellent Microwave Electromagnetic Properties. *Mater. Lett.* **2013**, *107*, 166−169.

(22) Liu, P. B.; Huang, Y.; Sun, X. Excellent Electromagnetic Absorption Properties of Poly(3,4-ethylenedioxythiophene)-Reduced Graphene Oxide−Co_3O_4 Composites Prepared by a Hydrothermal Method. *ACS Appl. Mater. Interfaces* **2013**, *5*, 12355−12360.

(23) Singh, V. K.; Shukla, A.; Patra, M. K.; Saini, L.; Jani, R. K.; Vadera, S. R.; Kumar, N. Microwave Absorbing Properties of a Thermally Reduced Graphene Oxide/nitrile Butadiene Rubber Composite. *Carbon* **2012**, *50*, 2202−2208.

(24) Fu, M.; Jiao, Q.; Zhao, Y. Preparation of $NiFe_2O_4$ Nanorod−graphene Composites via an Ionic Liquid Assisted One-step Hydrothermal Approach and Their Microwave Absorbing Properties. *J. Mater. Chem. A* **2013**, *1*, 5577−5586.

(25) Guo, J. L.; Chiou, Y. D.; Liang, W. I.; Liu, H. J.; Chen, Y. J.; Kuo, W. C.; Tsai, C. Y.; Tsai, K. A.; Kuo, H. H.; Hsieh, W. F.; Juang, J. Y.; Hsu, Y. J.; Lin, H. J.; Chen, C. T.; Liao, X. P.; Shi, B.; Chu, Y. H. Complex Oxide-Noble Metal Conjugated Nanoparticles. *Adv. Mater.* **2013**, *25*, 2040−2044.

(26) Zheng, H.; Wang, J.; Lofland, S. E.; Ma, Z.; Mohaddes-Ardabili, L.; Zhao, T.; Salamanca-Riba, L.; Shinde, S. R.; Ogale, S. B.; Bai, F.; Viehland, D.; Jia, Y.; Schlom, D. G.; Wuttig, M.; Roytburd, A.; Ramesh, R. Multiferroic $BaTiO_3$-$CoFe_2O_4$ Nanostructures. *Science* **2004**, *303*, 661−663.

(27) Ren, S.; Wuttig, M. Magnetoelectric Nano-Fe_3O_4/$CoFe_2O_4$||$PbZr_{0.53}Ti_{0.47}O_3$ Composite. *Appl. Phys. Lett.* **2008**, *92*, 083502.

(28) Peng, E.; Choo, E. S. G.; Chandrasekharan, P.; Yang, C. T.; Ding, J.; Chuang, K. H.; Xue, J. M. Synthesis of Manganese Ferrite/Graphene Oxide Nanocomposites for Biomedical Applications. *Small* **2012**, *8*, 3620−3630.

(29) Zhang, X. J.; Wang, G. S.; Wei, Y. Z.; Guo, L.; Cao, M. S. Polymer-composite with High Dielectric Constant and Enhanced Absorption Properties Based on Graphene−CuS Nanocomposites and Polyvinylidene Fluoride. *J. Mater. Chem. A* **2013**, *1*, 12115−12122.

(30) Wang, G. S.; Zhang, X. J.; Wei, Y. Z.; He, S.; Guo, L.; Cao, M. S. Polymer Composites with Enhanced Wave Absorption Properties Based on Modified Graphite and Polyvinylidene Fluoride. *J. Mater. Chem. A* **2013**, *1*, 7031−7036.

(31) He, S.; Wang, G. S.; Lu, C.; Liu, J.; Wen, B.; Liu, H.; Guo, L.; Cao, M. S. Enhanced Wave Absorption of Nanocomposites Based on the Synthesized Complex Symmetrical CuS Nanostructure and Poly(vinylidene fluoride). *J. Mater. Chem. A* **2013**, *1*, 4685−4692.

(32) Wang, G. S.; Wu, Y.; Wei, Y. Z.; Zhang, X. J.; Li, Y.; Li, L. D.; Wen, B.; Yin, P. G.; Guo, L.; Cao, M. S. Fabrication of Reduced Graphene Oxide (RGO)/Co_3O_4 Nanohybrid Particles and a RGO/Co_3O_4/Poly(vinylidene fluoride) Composite with Enhanced Wave-Absorption Properties. *ChemPlusChem.* **2014**, *79*, 375−381.

(33) Hummers, W. S.; Offeman, R. E. Preparation of Graphitic Oxide. *J. Am. Chem. Soc.* **1958**, *80*, 1339−1339.

(34) Bai, X.; Zhai, Y.; Zhang, Y. Green Approach To Prepare Graphene-Based Composites with High Microwave Absorption Capacity. *J. Phys. Chem. C* **2011**, *115*, 11673−11677.

(35) Wang, Y.; Cheng, R.; Wen, Z.; Zhao, L. Synthesis and Characterization of Single-Crystalline $MnFe_2O_4$ Ferrite Nanocrystals

and Their Possible Application in Water Treatment. *Eur. J. Inorg. Chem.* **2011**, *2011*, 2942−2947.
(36) Fan, D.; Zhang, C.; He, J.; Hua, R.; Zhang, Y.; Yang, Y. Redox Chemistry Between Graphene Oxide and Mercaptan. *J. Mater. Chem.* **2012**, *22*, 18564−18571.
(37) Sun, X.; He, J.; Li, G.; Tang, J.; Wang, T.; Guo, Y.; Xue, H. Laminated Magnetic Graphene with Enhanced Electromagnetic Wave Absorption Properties. *J. Mater. Chem. C* **2013**, *1*, 765−777.
(38) Zhang, Y.; Tian, J.; Li, H.; Wang, L.; Qin, X.; Asiri, A. M.; Al Youbi, A. O.; Sun, X. Biomolecule-Assisted, Environmentally Friendly, One-Pot Synthesis of CuS/Reduced Graphene Oxide Nanocomposites with Enhanced Photocatalytic Performance. *Langmuir* **2012**, *28*, 12893−12900.
(39) Lazarević, Z. Ž.; Jovalekić, Č.; Recnik, A.; Ivanovski, V. N.; Mitrić, M.; Romčević, M. J.; Paunović, N.; Cekić, B. Đ.; Romčević, N. Ž. Study of Manganese Ferrite Powders Prepared by a Soft Mechanochemical Route. *J. Alloys Compd.* **2011**, *509*, 9977−9985.
(40) Lin, X.; Lv, X.; Wang, L.; Zhang, F.; Duan, L. Preparation and Characterization of $MnFe_2O_4$ in the Solvothermal Process: Their Magnetism and Electrochemical Properties. *Mater. Res. Bull.* **2013**, *48*, 2511−2516.
(41) Zhou, W.; Hu, X.; Bai, X.; Zhou, S.; Sun, C.; Yan, J.; Chen, P. Synthesis and Electromagnetic, Microwave Absorbing Properties of Core−Shell Fe_3O_4−Poly(3, 4-ethylenedioxythiophene) Microspheres. *ACS Appl. Mater. Interfaces* **2011**, *3*, 3839−3845.
(42) Wang, C.; Han, X.; Zhang, X.; Hu, S.; Zhang, T.; Wang, J.; Du, Y.; Wang, X.; Xu, P. Controlled Synthesis and Morphology-Dependent Electromagnetic Properties of Hierarchical Cobalt Assemblies. *J. Phys. Chem. C* **2010**, *114*, 14826−14830.
(43) Wang, G. S.; Nie, L. Z.; Yu, S. H. Tunable Wave Absorption Properties of β-MnO_2 Nanorods and their Application in Dielectric Composites. *RSC Adv.* **2012**, *2*, 6216−6221.
(44) Cao, M. S.; Shi, X. L.; Fang, X. Y.; Jin, H. B.; Hou, Z. L.; Zhou, W.; Chen, Y. J. Microwave Absorption Properties and Mechanism of Cagelike ZnO/SiO_2 Nanocomposites. *Appl. Phys. Lett.* **2007**, *91*, 203110.
(45) Xu, B.; Wang, C.; Hu, S.; Han, X.; Huang, W.; Tian, L. Controlled Synthesis and Microwave Absorption Property of Chain-Like Co Flower. *PLoS One* **2013**, *8*, e55928.
(46) Wang, D.; Zhang, X.; Zha, J. W.; Zhao, J.; Dang, Z. M.; Hu, G. H. Dielectric Properties of Reduced Graphene Oxide/polypropylene Composites with Ultralow Percolation Threshold. *Polymer* **2013**, *54*, 1916−1922.
(47) Xu, H. P.; Dang, Z. M.; Jiang, M. J.; Yao, S. H.; Bai, J. Enhanced Dielectric Properties and Positive Temperature Coefficient Effect in the Binary Polymer Composites with Surface Modified Carbon Black. *J. Mater. Chem.* **2008**, *18*, 229−234.
(48) Liu, T.; Zhou, P. H.; Xie, J. L.; Deng, L. J. The Hierarchical Architecture Effect on the Microwave Absorption Properties of Cobalt Composites. *J. Appl. Phys.* **2011**, *110*, 033918.
(49) Wang, C.; Han, X.; Xu, P.; Zhang, X.; Du, Y.; Hu, S.; Wang, J.; Wang, X. The Electromagnetic Property of Chemically Reduced Graphene Oxide and its Application as Microwave Absorbing Material. *Appl. Phys. Lett.* **2011**, *98*, 072906.
(50) Wang, G. S.; Wei, Y. Z.; Lu, C.; Yue, Y. H.; Wu, J.; Guo, L. Bioinspired Design and Assembly of Platelet Reinforced Polymer Films with Enhanced Absorption Properties. *J. Mater. Chem. A* **2014**, *2*, 5516−5524.
(51) Wang, G. S.; He, S.; Luo, X.; Wen, B.; Lu, M. M.; Guo, L.; Cao, M. S. Synthesis and Growth Mechanism of 3D α-MnO_2 Clusters and Their Application in Polymer Composites with Enhanced Microwave Absorption Properties. *RSC Adv.* **2013**, *3*, 18009−18015.
(52) van der Zaag, P. J. New Views on the Dissipation in Soft Magnetic Ferrites. *J. Magn. Magn. Mater.* **1999**, *196−197*, 315−319.
(53) Liu, X. G.; Li, B.; Geng, D. Y.; Cui, W. B.; Yang, F.; Xie, Z. G.; Kang, D. J.; Zhang, Z. D. (Fe, Ni)/C Nanocapsules for Electromagnetic-wave-absorber in the Whole Ku-band. *Carbon* **2009**, *47*, 470−474.
(54) Guo, J.; Wang, X.; Miao, P.; Liao, X.; Zhang, W.; Shi, B. One-step Seeding Growth of Controllable Ag@Ni Core−shell Nanoparticles on Skin Collagen Fiber with Introduction of Plant Tannin and Their Application in High-performance Microwave Absorption. *J. Mater. Chem.* **2012**, *22*, 11933−11942.
(55) Zhu, J.; Wei, S.; Haldolaarachchige, N.; Young, D. P.; Guo, Z. Electromagnetic Field Shielding Polyurethane Nanocomposites Reinforced with Core−Shell Fe−Silica Nanoparticles. *J. Phys. Chem. C* **2011**, *115*, 15304−15310.